Insect Biochemistry and Molecular Biology 108 (2019) 44–52

Contents lists available at ScienceDirect

Insect Biochemistry and Molecular Biology

journal homepage: www.elsevier.com/locate/ibmb

The three-dimensional structure and recognition mechanism of *Manduca sexta* peptidoglycan recognition protein-1

Yingxia Hu[1,2], Xiaolong Cao[1,2], Xiuru Li[3], Yang Wang[1], Geert-Jan Boons[3,d,e], Junpeng Deng[2,**], Haobo Jiang[1,*]

[1] Department of Entomology and Plant Pathology, Oklahoma State University, Stillwater, OK, 74078, USA
[2] Department of Biochemistry and Molecular Biology, Oklahoma State University, Stillwater, OK, 74078, USA
[3] Complex Carbohydrate Research Center, University of Georgia, Athens, GA, 30602, USA
[d] Department of Chemistry, University of Georgia, Athens, GA, 30602, USA
[e] Chemical Biology and Drug Discovery, Utrecht Institute for Pharmaceutical Sciences, Bijvoet Center for Biomolecular Research, Utrecht University, 3584 CG, Utrecht, the Netherlands

ARTICLE INFO

Keywords:
Insect immunity
Pattern recognition
Hemolymph protein
Serine protease
Prophenoloxidase activation
Melanization

ABSTRACT

Peptidoglycan recognition proteins (PGRPs) recognize bacteria through their unique cell wall constituent, peptidoglycans (PGs). PGRPs are conserved from insects to mammals and all function in antibacterial defense. In the tobacco hornworm *Manduca sexta*, PGRP1 and microbe binding protein (MBP) interact with PGs and hemolymph protease-14 precursor (proHP14) to yield active HP14. HP14 triggers a serine protease network that produces active phenoloxidase (PO), Spätzle, and other cytokines to stimulate immune responses. PGRP1 binds preferentially to diaminopimelic acid (DAP)-PGs of Gram-negative bacteria and Gram-positive *Bacillus* and *Clostridium* species than Lys-PGs of other Gram-positive bacteria. In this study, we synthesized DAP- and Lys-muramyl pentapeptide (MPP) and monitored their associations with *M. sexta* PGRP1 by surface plasmon resonance. The K_d values (0.57 μM for DAP-MPP and 45.6 μM for Lys-MPP) agree with the differential recognition of DAP- and Lys-PGs. To reveal its structural basis, we produced the PGRP1 in insect cells and determined its structure at a resolution of 2.1 Å. The protein adopts a fold similar to those from other PGRPs with a classical L-shaped PG-binding groove. A unique loop lining the shallow groove suggests a different ligand-binding mechanism. In summary, this study provided new insights into the PG recognition by PGRPs, a critical first step that initiates the serine protease cascade.

1. Introduction

Recognition of microbe-associated molecular patterns is critically important for a successful innate immune response against pathogen invasion. Pattern recognition receptors have evolved in insects to specifically bind peptidoglycans, β-1,3-glucans and other surface components of bacteria and fungi (Jiang et al., 2010; Kurata, 2014). Clustering of pattern recognition receptors on the microbial surface triggers a serine protease system that activates cytokines (*e.g.* Spätzle) and phenoloxidase (PO) to induce antimicrobial peptide (AMP) synthesis, stimulate cellular responses, and kill the infectious agents (Kanost and Jiang, 2015; Lemaitre and Hoffmann, 2007; Strand, 2008).

Peptidoglycans (PGs) are unique and essential components of walled bacteria, with repetitive structures eliciting innate immune responses of vertebrate and invertebrate hosts (Guan and Mariuzza, 2007). Their glycan strands of alternating β-1,4-linked *N*-acetylglucosamine and *N*-acetylmuramate (NAM) are attached with peptide stems of 3–5 amino acids via the lactyl group on some NAM residues. The adjacent stems are cross-linked either directly or through a short peptide bridge to form a mesh-like PG layer (Vollmer et al., 2008). The polysaccharide chain is conserved in all bacteria, but the stem peptides vary in amino acid composition as well as degree of cross-linking. Gram-negative bacteria and Gram-positive bacteria in the genera of *Bacillus* and *Clostridium* contain *meso*-diaminopimelate (DAP) as the third residue of the stems, whereas other Gram-positive bacteria have a Lys at the same position (Vollmer et al., 2008).

Abbreviations: AMP, antimicrobial peptide; DAP, diaminopimelate; MBP, microbe binding protein; MPP, muramyl pentapeptide; NAM, *N*-acetylmuramate; PG and PGRP, peptidoglycan and its recognition protein; PO and proPO, phenoloxidase and its precursor; proHP14, hemolymph protease-14 precursor

* Corresponding author.Dept. Entomol. & Plant Pathol, Oklahoma State University, Stillwater, OK, 74078, USA.
** Corresponding author.Dept. Biochem. & Mol. Biol, Oklahoma State University, Stillwater, OK 74078, USA.
E-mail addresses: Junpeng.deng@okstate.edu (J. Deng), haobo.jiang@okstate.edu (H. Jiang).

https://doi.org/10.1016/j.ibmb.2019.03.001
Received 25 October 2018; Received in revised form 26 January 2019; Accepted 1 March 2019
Available online 21 March 2019
0965-1748/

Peptidoglycan recognition proteins (PGRPs) bind to PGs and regulate antimicrobial responses ranging broadly from arthropods to mammals (Dziarski, 2004; Dziarski and Gupta, 2006). All PGRP family members adopt a conserved protein architecture similar to that from bacteriophage T7 lysozyme, containing an N-terminal segment with varying lengths and a C-terminal PG-binding domain of about 165 amino acid residues. Similar to T7 lysozyme (Cheng et al., 1994), some PGRPs possess a Zn-dependent amidase activity by hydrolyzing the bond between lactyl and Ala at position-1 of the stems on PGs and generate non-immunogenic fragments. These PGRPs are hence classified as catalytic PGRPs (Gelius et al., 2003; Kim et al., 2003; Mellroth et al., 2003; Wang et al., 2003). However, most PGRPs lack the amidase activity and only act as receptors for ligand-dependent signaling (Werner et al., 2000). Some of the *Drosophila* and human PGRP structures contain monomeric DAP- or Lys-PG, indicating that several residues may be involved in differential recognition of DAP- and Lys-PGs (Chang et al., 2005, 2006; Cho et al., 2007; Guan et al., 2004, 2006; Kim et al., 2003; Leone et al., 2008; Lim et al., 2006; Reiser et al., 2004).

In the tobacco hornworm *Manduca sexta*, 5 PGRPs are up-regulated upon microbial challenge (Zhang et al., 2015). PGRP1 acts as a sensor of the prophenoloxidase (proPO) activation system, which binds to soluble DAP-PG of *Escherichia coli* and insoluble PGs from various Gram-negative and certain Gram-positive bacteria, but not to soluble Lys-PG of *Staphylococcus aureus* (Sumathipala and Jiang, 2010). The differential recognition of DAP- and Lys-type PGs is in fact common across the PGRP family (Swaminathan et al., 2006). Our recent study showed that PGRP1 along with microbe binding protein (MBP) interacts with PGs, which lead to the autoactivation of hemolymph protease-14 precursor (proHP14) to yield active HP14 that initiates the proPO activation system in a Ca^{2+}-dependent manner (Wang and Jiang, 2017). The proPO activation in response to specific recognition of bacterial PGs is remarkably sensitive. In fact, this phenomenon has led to the development of a commercial kit for detecting bacterial contamination of human platelet units, by using *M. sexta* hemolymph as the key component (Heaton et al., 2014).

To understand the mechanism of PG recognition by PGRP1, we expressed and purified *M. sexta* PGRP1 from Sf9 insect cells and determined its crystal structure to 2.1 Å resolution, which represents the first PGRP structure from Lepidoptera. Through structural comparison with other known PGRP structures, we have identified unique structural features of its PG-binding pocket, providing insights into the recognition mechanism of PGRPs.

2. Materials and methods

2.1. Expression and purification of M. sexta PGRP1

As described previously (Sumathipala and Jiang, 2010), a recombinant baculovirus stock ($1-2\times10^8$ pfu/ml) was prepared from the PGRP1 bacmid for infecting Sf9 cells at 2.4×10^6 cells/ml in 1000 ml of Sf-900™ III serum-free medium at a multiplicity of infection of 5–8. At 72 h after infection, the cell culture was centrifuged at $2500\times g$ for 20 min, diluted with 1.0 l of 1.0 mM benzamidine, and centrifuged at $20{,}000\times g$ rpm for 30 min. The supernatant was loaded onto a dextran sulfate-Sepharose column (80 ml) equilibrated with buffer A (10 mM potassium phosphate, pH 6.2). After washing with 400 ml of buffer A, bound proteins were eluted with a linear gradient of 0–1.0 M NaCl in buffer A (400 ml) and 1.0 M NaCl in buffer A (200 ml) to ensure complete elution. Aliquots of the column fractions (8.0 ml/tube) were subjected to 12% SDS-PAGE, staining and immunoblot analysis using 1:2000 diluted rabbit antiserum to PGRP1. The pooled PGRP1 fractions were loaded onto a 5 ml Ni-NTA agarose column equilibrated with buffer B (50 mM potassium phosphate, 0.3 M NaCl, 0.01% Tween-20, pH 8.0). After washing with 75 ml of buffer B containing 10 mM imidazole, the bound PGRP1 was eluted with a linear gradient of 10–100 mM imidazole in buffer B (150 ml) and 250 mM imidazole in buffer B (50 ml). After SDS-PAGE, staining and immunoblot analysis, fractions (3.0 ml/tube) containing pure PGRP1 were pooled, concentrated and buffer exchanged to a final concentration of 8.0 mg/ml in 20 mM Tris-HCl, 500 mM NaCl, pH 7.5. The protein aliquots were flash frozen and stored at −80 °C until usage for optimal reproducibility of crystallization (Deng et al., 2004).

2.2. Chemical synthesis of DAP- and Lys-muramyl pentapeptides

The synthesis of DAP-MPP and Lys-MPP was carried out on Sieber amide resin (0.25 mmol) using Fmoc chemistry as previously described (Kumar et al., 2005). Fmoc-D-Ala-OH (26.12 mg, 84 μmol) in DMF was coupled with Sieber amide resin (100 mg, 42 μmol) after treated with 20% piperidine in 2 ml DMF for 5 min three times and washed with 3 ml of freshly distilled DMF three times by using benzotriazole-1-yl-oxy-tris-pyrrolidino-phosphonium hexafluorophosphate (43.7 mg, 0.08 mmol), 1-hydroxybenzotriazole (11 mg, 0.08 mmol), and diisopropylethylamine (29.2 μl, 0.16 μmol) as the activating reagents. Progress of the reaction was monitored by the Kaiser test. After completion of the coupling, the resin was washed with 3 ml of DMF three times, and the Fmoc protecting group was removed with 20% piperidine in DMF (2 ml, 5 min, 3 times). The reaction cycle was repeated using 84 μmol of Fmoc-D-Ala-OH, Fmoc-L-Lys(Mtt)-OH, Fmoc-D-isoglutamine, Fmoc-L-Ala-OH and 2-*N*-acetyl-1-β-*O*-allyl-4,6-benzylidene-3-muramic acid sequentially. The resulting resin-bound glycopeptide was washed with 3 ml of DMF 3 times, dichloromethane (DCM) 7 times, and methanol 3 times followed by drying *in vacuo* for 4 h. The resin was re-swelled in 5 ml of DCM and filtered, then treated with 2 ml of 2% trifluoroacetic acid (TFA) in DCM 10 times to release the glycopeptides from the resin. The combined washings were concentrated under reduced pressure and co-evaporated with 10 ml of toluene 3 times to remove traces of TFA. The crude product was subjected to 20% TFA in DCM to ensure complete removal of the benzylidene protecting group. The resulting product was purified by size exclusion chromatography on a Sephadex G15 column (Amersham Biosciences). The yielded compound (allyl-2-*N*-acetyl-3-*O*-muramyl)-L-alanyl-D-isoglutamyl-L-lysine was dissolved in a mixture of ethanol/acetic acid/water (2:1:1, 0.8 ml) and added 10% palladium on activated charcoal (9 mg). After stirring for 48 h at room temperature, the reaction mixture was filtered, the filtrate was concentrated under reduced pressure, the residue was co-evaporated from toluene, and the target compound Lys-MPP was separated from other compounds on the Sephadex G15 column. DAP-MPP was synthesized using a similar protocol except for the substitution of Fmoc-L-Lys(Mtt)-OH with Fmoc-DAP (BOC, tBu)-OH (Chowdhury and Boons, 2005). The M_r's of Lys- and DAP-MPP were determined by high-resolution MALDI-TOF mass spectrometry.

2.3. Measurement of DAP- or Lys-MPP binding to M. sexta PGRP1 by surface plasmon resonance (SPR)

Binding interactions between PGRP1 and the ligands were examined using a Biacore T100 biosensor system (Biacore Inc. GE Healthcare). The protein was immobilized by standard amine coupling using an amine coupling kit (Biacore Inc. GE Healthcare). Briefly, the surface was activated with 1:1 (v/v) freshly mixed *N*-hydroxysuccimide (NHS, 100 mM) and 1-(3-dimethylaminopropyl)-ethylcarbodiimide (EDC; 391 mM) in water. Next, PGRP1 (50 μg/ml) in 10 mM NaOAc (pH 5.0) was passed over the chip surface until a ligand density of approximately 3000 RU was achieved. The remaining active esters were quenched by 1.0 M ethanolamine (pH 8.5) in water. The control flow cell was activated with NHS and EDC followed by immediate quenching with ethanolamine. HBS-EP (pH 7.4, 0.01 M HEPES, 150 mM NaCl, 3 mM EDTA, 0.005% polysorbate 20) was used as running buffer for immobilization and kinetic studies. Analytes dissolved in the running buffer was employed at a flow rate of 30 μL/min for association and

dissociation at a constant temperature of 25 °C. A 60 s injection of 10 mM NaOH (pH 9.4) was used at 30 µl/min for regeneration and achieving prior baseline status. Using Biacore T100 evaluation software, the response curves of analytes at various concentrations were globally fitted to the 1:1 binding model.

2.4. Protein crystallization

Crystallization screening was performed at room temperature by sitting drop vapor diffusion method on 96-well Intelli-plates (Art Robbins Instruments). The initial trials were set up using commercial kits including Crystal Screen I and II, Index, PEG/Ion, SaltRx (Hampton), Wizard I, II, III, IV (Emerald Biosystems), JCSG I, II, III, IV (QIAGEN). Concentrated PGRP1 (0.5 µl) was mixed with crystallization reagents at a 1:1 v/v ratio in a well against a reservoir containing 75 µl of the reagent. PGRP1 crystals formed as plate clusters with a reservoir solution of 0.2 M ammonium chloride, 20% (w/v) PEG 3350, pH 6.3. A single plate of crystal was manually isolated, and 20% glycerol was used as cryoprotectant during flash freezing of the crystal in liquid nitrogen.

2.5. Data collection and structural determination

One set of data was collected at 100 K to 2.10 Å resolution at Advanced Photon Source, beamline 19-ID, Argonne National Laboratory (Argonne, IL) and processed using HKL3000 program (Minor et al., 2006). The initial phasing was obtained by molecular replacement using the Phaser program of CCP4 suite, in which chain A of the crystal structure of *Drosophila melanogaster* PGRP-SA (PDB code 1S2J) was used as the searching model. Subsequent model building was carried out using Autobuild program of Phenix (Adams et al., 2010) coupled with manual modeling using WinCoot (Emsley et al., 2010). The structure was further refined using Phenix. The current structure model is of excellent geometry and refinement statistics (Table I), and validated by wwpdb validation servers (Berman et al., 2003) and with the Molprobity server (Chen et al., 2010). All structural figures were generated using PyMol (DeLano, 2002).

Table 1
Data collection and refinement statistics.

Crystal data	
Beam-line	19-ID APS
Wavelength, Å	0.97915
Space group	C 1 2 1
Cell constants	a = 63.7 Å, b = 46.4 Å, c = 62.4 Å, β = 103.1°
Resolution, Å	2.10
Total reflections	39,115
Unique reflections	10,140
Completeness, %	96.9 (89.7)
I/σ	9.4 (2.5)
R_{sym}, %	13.2 (37.9)
Refinement statistics	
Reflection range used, Å	2.10–33.83
No. reflections used	10,135
R_{work}/R_{free}, %	18.0/22.0
rmsd bonds, Å	0.0047
rmsd angle, °	0.701
Ramachandran plot (preferred/allowed/outlier), %	98.3/1.1/0.6
No. atoms	
Protein	1400
Waters	177

$R_{sym} = \Sigma|I_{obs} - I_{avg}|/\Sigma I_{avg}$; $R_{work} = \Sigma \; | \; |F_{obs} - F_{calc}| \; | / \Sigma F_{obs}$.
R_{free} was calculated using 5% data.
APS, Advanced Photon Source; I/σ, Intensity/Sigma (Intensity). Values in parentheses are for the highest-resolution shell 2.18–2.10 Å.

2.6. Docking analysis

The docking of DAP- and Lys-MPP into the PG-binding groove of *M. sexta* PGRP1 was performed using AutoDock (version 4.2.6) (Morris et al., 2009). The structure of DAP-MPP was modified from the Lys-MPP ligand bound to human PGRP-Iα (PDB ID 2APH), by adding an ε-carboxyl group at the side chain of Lys. Based on structural analyses of the other PGRPs in complex with PG monomers (Chang et al., 2005, 2006; Cho et al., 2007; Guan et al., 2004; Lim et al., 2006), N60, Y61, N89, Y90, Y92, H140, L144 of PGRP1 were selected as flexible residues and all of the bonds between CA and CB were inactivated, to allow slight protein dynamics upon substrate binding. Most of the bonds in DAP-MPP were also inactivated, leaving CA-C and CG-CD of D-isoGln, N-CA, CA-CB, CA-C, CD-CE and CE-C02 of DAP, N-CA and CA-C of D-Ala, N-CA and CA-C of the C-terminal D-Ala rotatable. Lamarckian genetic algorithm (LGA) with 2,500,000 evaluations per run was chosen as the searching method. Default settings were used for all other docking parameters. The docked conformations with the lowest docking energy for two types of binding were selected for analysis.

3. Results and discussion

3.1. Binding properties of the recombinant M. sexta PGRP1

We chemically synthesized the monomeric Lys- and DAP-PGs to study their interactions with *M. sexta* PGRP1 (Fig. 1). As determined by MALDI-TOF mass spectrometry, the observed M_r's (784.7832 and 828.7411 Da) were identical to the theoretical values of Lys-MPP ($C_{31}H_{55}N_9O_{13}Na$ [M + Na]: 784.8308 Da) and DAP-MPP ($C_{32}H_{55}N_9O_{15}Na$ [M + Na]: 828.8398 Da). SPR was used to examine the binding affinity and kinetics of recombinant *M. sexta* PGRP1 with the ligands. PGRP1 was immobilized on a CM5 sensor chip whereas the PG monomers at various concentrations were flowed through the chip. The sensorgrams were collected to calculate the corresponding dissociation constant (K_d) (Fig. 1). The K_d for Lys-MPP (45.58 µM, fitting parameter Chi^2: 0.184 RU^2) were 80 times as high as that for DAP-MPP (0.57 µM, Chi^2: 0.503 RU^2). In other words, the binding of DAP-MPP is much stronger than Lys-MPP, consistent with the previous finding that *M. sexta* PGRP1 binds preferably to polymeric DAP-PGs than Lys-PGs and triggers melanization (Sumathipala and Jiang, 2010). The binding constants of DAP-type and Lys-type PGs for *M. sexta* PGRP1 are similar to those for the other DAP-type PGRPs (Table S1).

3.2. Overview of the PGRP1 structure

The crystal structure of *M. sexta* PGRP1 contains one subunit in the asymmetric unit with a dimension of about 48 × 36 × 39 Å (Fig. 2A). In the final refined model, residue 1 is disordered and residues 2–172 (Cys − Asp) are well defined with clearly interpretable electron densities. Residues 1–24 (Asp − Pro) belong to the N-terminal PGRP-specific segment and residues 25–172 (Ile − Asp) constitute the PGRP domain homologous to the T7 lysozyme. The overall structure is composed of a central β sheet flanked by four α-helices and three β-turns. The conserved central β sheet is made up of five β strands, four parallel (β1, 2, 4, 5) and one anti-parallel (β3). The overall structure of PGRP1 resembles those of *Drosophila* and human PGRPs (RMSDs over Cα atoms: 0.603–0.773 Å) (Fig. 2B). The greatest difference lies in the C-termini, in which *M. sexta* PGRP1 contains a fourth α-helix, whereas the corresponding regions from all other PGRPs adopt a flexible loop. Other differences are present in the N-termini and β turn regions. *Drosophila* PGRP-LB and -LE (Kim et al., 2003; Lim et al., 2006) have two extra β strands at the N-termini, one as a part of the six-stranded central β sheet and the other within the PGRP-specific segment. In the other PGRPs including *M. sexta* PGRP1, the two β strands are replaced by flexible loops. Besides, the numbers of β turns vary among the PGRPs (three in *M. sexta* PGRP1), some missing or substituted with

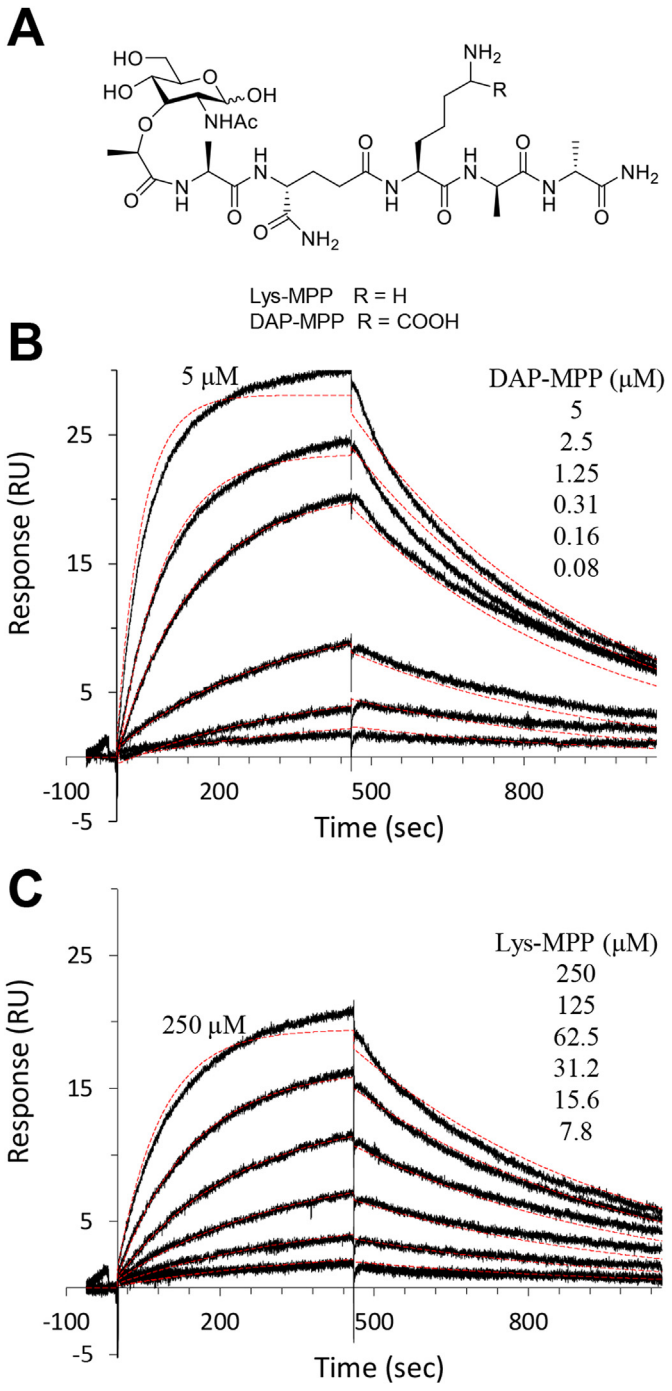

Fig. 1. Structures of Lys- and DAP-MPPs and sensorgrams of their binding to *M. sexta* PGRP1. (**A**) Chemical structure; (**B**, **C**) SPR sensorgrams. PGRP1 was covalently linked to the sensor chip. At 0 s, Lys- or DAP-MPP at various concentrations (see *insets*) was flowed over the chip, followed by a buffer only dissociation step (Section 2.3). Positive deflection of the curve indicates binding in resonance units (RUs). The primary data (*black* lines) were fitted with a 1:1 binding model, as indicated by *red dashed* lines. (For interpretation of the references to color in this figure legend, the reader is referred to the Web version of this article.)

random coils.

M. sexta PGRP1 contains two disulfide bonds (Cys38-Cys44 and Cys2-Cys124) that contribute to the structural integrity (Fig. 2). Cys38 and Cys44 form a buried bridge tethering helix α1 to the central β-sheet. This bond is highly conserved among all known PGRP structures except *Drosophila* PGRP-LE. Disruption of the disulfide bond in *Drosophila* PGRP-SA by mutagenesis abolished the Toll pathway activation by Gram-positive bacteria (Michel et al., 2001), indicating its importance in the PG recognition or conformational change in PGRP-SA. The bond between Cys2 and Cys124 connects the N-terminus to α2 helix and these two residues are located at the opposite side of the PG-binding groove, exposed to the solvent. This disulfide bridge is present in all the available structures of mammalian PGRPs, as well as *Drosophila* PGRP-SA. Mammalian PGRPs possess a third disulfide bond at the lower side of the PG-binding groove, which is absent in all the insect PGRPs.

3.3. Active site

Bacteriophage T7 lysozyme and *Drosophila* PGRP-LB both have an amidase activity; both contain a required zinc ion at the active site (Cheng et al., 1994; Kim et al., 2003). The Zn^{2+} ion is coordinated with one Cys and two His residues. *M. sexta* PGRP1 lacks two of the three residues, with Ser148 aligned to the Cys and Gln31 to one His residue (Fig. 3A). The electron density at the Zn^{2+}-equivalent site fits a water molecule rather than a zinc ion (Fig. 3B), and the water is hydrogen bonded with the side chains of Gln31, His140 and Ser148. Considering the culture medium contains sufficient Zn^{2+} ions, the absence of Zn^{2+} in the structure suggests that *M. sexta* PGRP1 is not a zinc-dependent amidase, consistent with the prediction based on sequence alignment (Sumathipala and Jiang, 2010).

However, a zinc-independent serine hydrolase activity cannot be excluded for *M. sexta* PGRP1. In *Drosophila* PGRP-SA, two catalytic mechanisms of serine hydrolase have been proposed. Mechanism I involves a modified catalytic triad composed of a Ser158/His41 juxtaposition, with the hydroxyl group of Thr99 and carbonyl oxygen of His98 contributing as the carboxyl group of a canonical acidic residue Asp or Glu (Fig. 4A) (Reiser et al., 2004). Mechanism II involves a Ser158/His42 catalytic dyad for an intrinsic L,D-carboxylpeptidase activity of *Drosophila* PGRP-SA (Fig. 4B) (Chang et al., 2004). Single mutation of S158C or H42A abolished the enzyme activity but not DAP-PG binding, indicating their roles in catalysis rather than recognition. In both mechanisms, Ser158 serves as the nucleophile, which is highly conserved among receptor-type PGRPs including *M. sexta* PGRP1 (Ser148, Fig. 4A and B). This Ser residue aligns to the zinc-coordinated Cys residue in PGRPs with amidase activities. Mechanism I seems unlikely for *M. sexta* PGRP1 because the other catalytic components are absent. His41 is replaced by Gln31 in PGRP1 and residues in this position are highly variable among PGRPs. His140 is located in the proximity of Ser148, but no nearby residues can act as an acid to form a catalytic triad. However, mechanism II is plausible as the proposed catalytic dyad does exist in *M. sexta* PGRP1 (Ser148-His32) (Fig. 4B), which is conserved among the non-amidase PGRPs. Ser148 and His32 are colocalized with a distance of about 4.5 Å, and interact with each other mainly through van der Waals forces. It is likely further induced fine changes of their conformations could occur upon substrate binding, allowing the catalysis to occur. Moreover, Asp34 from another loop, a unique residue in the PGRP1 near the dyad, may serve as an acid to facilitate the catalysis after it approaches His32. This conserved Ser/His dyad along with Asp34 resides on top of the PG-binding groove close to the zinc site of amidase PGRPs, and are easy for the PG substrate to access (Fig. 4C). In order to test the proposed catalytic activity, we incubated PGRP1 with either PG monomers or PG polymer fragments generated by lysozyme digestion and examined the cleavage products by mass spectrometry. While no cleavage occurred in the synthetic compounds (data not shown), we detected 50–80 new mass peaks after PGRP1 had been added to the lysozyme-treated *E. coli* and *S. aureus* PGs (Fig. S1). Unfortunately, we have failed to assign their masses to the predicted products but consider the catalytic function of *M. sexta* PGRP1 worth exploring in the future.

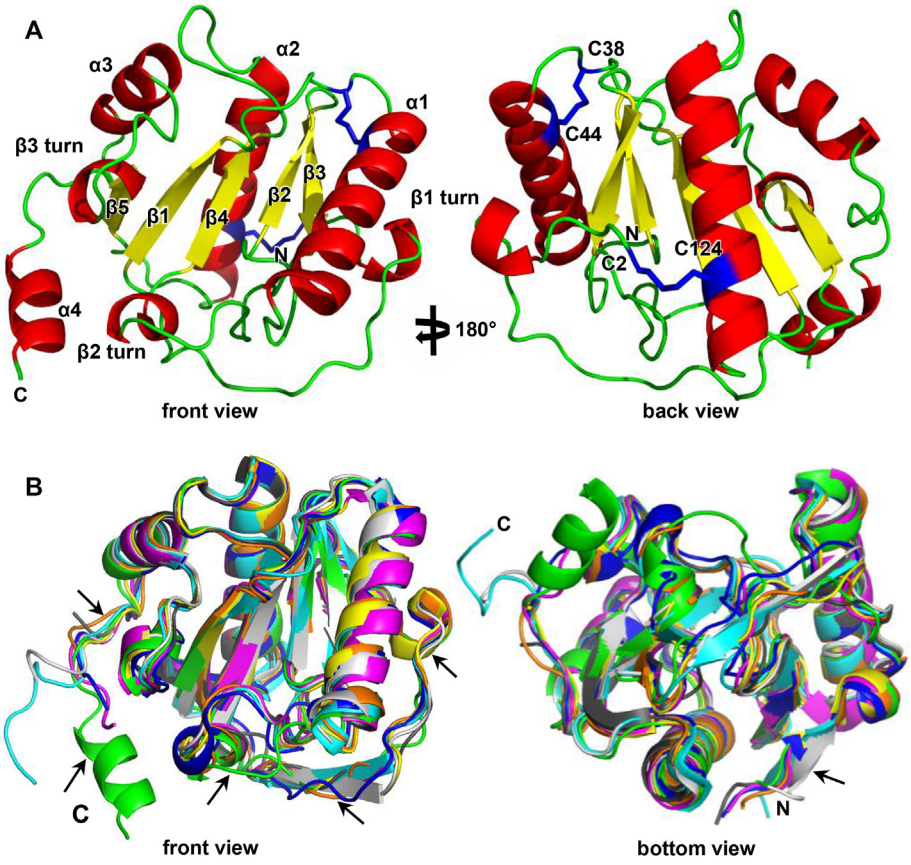

Fig. 2. Crystal structure of *M. sexta* PGRP1. (**A**) Overall structure of the PGRP1. The secondary structures are colored as following: α-helix and β turn, *red*; β strand, *yellow*; loop, *green*; disulfide bond, *blue stick*. (**B**) Superposition of *M. sexta* PGRP1 (6CKH, *green*) with *Drosophila* PGRP-LB (1OHT, *cyan*), -LCx (2F2L-X, *yellow*), -LE (2CB3, *silver*), -SA (1S2J, *magenta*), -SD (2RKQ, *blue*), human PGRP-S (1YCK, *orange*), -Iα (1SK3, *dark gray*). RMSDs over Cα atoms of the PGRP1 and other PGRPs are 0.603–0.773 Å. Differences in secondary structures are indicated by *arrows*. (For interpretation of the references to color in this figure legend, the reader is referred to the Web version of this article.)

3.4. PG-binding groove

M. sexta PGRP1 contains a classical L-shaped PG-binding groove, which comprises a deep area and a shallow region (Fig. 5A). The deep area consists of the central β sheet, especially β1, β4 and β2, and flanked by the β3-turn along with its subsequent loop, the β1-α1 loop and C-terminal part of α1 (Fig. 2). The base of this area is much deeper than those from other PGRPs' (data not shown). The shallow region is delineated by β2-turn as well as part of its preceding loop. The groove is predominantly hydrophilic and filled with water molecules. Overall, the surface residues in the groove are more conserved than those in the rest of the molecule; within the groove, residues on the floor are relatively more conserved than those lining the wall (Fig. 5B).

In the crystal structure of *Drosophila* PGRP-LCa ectodomain, which is deficient in binding to the monomeric PG on its own, the classical PG-binding groove is disrupted by two unique helical insertions (Chang et al., 2005). The first one locates in the shallow region and mainly consists of Asn442 and Met441 from the α3/L3 loop, whose conformation is believed to be affected by the α3 helix. Interestingly, this short helix also exists in *M. sexta* PGRP1, however as the β2-turn (Fig. 6A). The preceding loop adopts a conformation completely different from that of *Drosophila* PGRP-LCa, resulting in a narrowed but undisrupted shallow region (Fig. 6B). This agrees with the result of functional tests that *M. sexta* PGRP1 is capable of binding PG ligands (Sumathipala and Jiang, 2010). Superposition of the structure of PGRP1 with those from known PGRP structures reveals a unique structural feature in PGRP1. Other members with or without the short helix/β2-turn all adopt a similar conformation as *Drosophila* PGRP-LCa at this particular loop region, with the only difference located at the insert portion (Fig. 6C). This unique loop region is mainly composed of Val87, Pro88, Asn89 and Tyr90, with the side chains of Asn89 and Tyr90 protruding from the surface (Fig. 6D). Most atoms of these four residues have comparable B factor values as those of other residues in the structure (Fig. S2), indicating this loop region is quite stable and well-ordered.

3.5. Identification of potential PG-binding residues in M. sexta PGRP1

It has been shown that PGRPs can discriminate PGs from different bacteria species (Swaminathan et al., 2006), most likely through distinct features of their stem peptides, such as amino acid composition, crosslinking degree, and accessibility of PGs in the cell wall. DAP differs from Lys only with an extra carboxyl group in the side chain, which is distinguished by some PGRPs. According to the structures of PG-bound PGRPs (Chang et al., 2006; Cho et al., 2007; Guan et al., 2004, 2006; Lim et al., 2006), the sugar moiety is always anchored in the deep area while the stem peptide spans the rest of the groove. In particular, several residues in the shallow region may participate in the differential recognition of DAP- and Lys-PGs (Fig. 7A), as proposed in these papers. Human PGRP-Iα binds monomeric DAP- and Lys-PGs with similar affinities (Kumar et al., 2005). In the crystal structure of human PGRP-Iα in complex with Lys-muramyl tri(T)/penta(P)-peptide, Asn236-Phe237 (NF) form intimate contacts with the side chain of Lys in the MTP or MPP through van der Waals interactions and hydrogen bonds (Guan et al., 2004, 2006). In *Drosophila* PGRP-SA and SD which activate the Toll pathway mainly in response to Gram-positive bacteria (Bischoff et al., 2004; Michel et al., 2001), Asp-Phe (DF) and Lys-Phe (KF) are located at the positions of NF respectively. In comparison, *Drosophila* PGRP-LCx, -LE and human PGRP-S which bind specifically to DAP-PGs (Kaneko et al., 2004; Kumar et al., 2005; Takehana et al., 2002) and *Drosophila* PGRP-LB which specifically hydrolyzes DAP-PGs (Zaidman-Remy et al., 2006), all contain Gly-Trp (GW) rather than NF. Tracheal cytotoxin (TCT)-bound *Drosophila* PGRP-LC and LE complex structures verified the van der Waals interactions between the particular Trp residue and DAP in the PG monomer (Chang et al., 2006; Lim et al., 2006). Surprisingly, *M. sexta* PGRP1 has Asn-Tyr (NY) at these sites

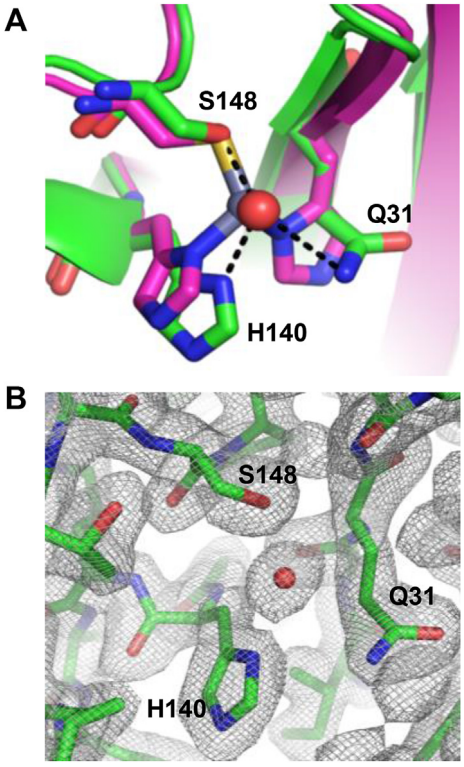

Fig. 3. *M. sexta* PGRP1 is not a zinc-dependent amidase that hydrolyzes PGs. (**A**) Superposition of the PGRP1 (6CKH, *green*) with the zinc centers of *Drosophila* PGRP-LB (1OHT, *magenta*). Zn^{2+}-coordinating residues of PGRP-LB along with the corresponding residues (labeled) in *M. sexta* PGRP1 are shown as *sticks*. Zn^{2+} ion and water molecules are shown as *gray* and *red spheres*, respectively, with the hydrogen bonds marked as *black dashes*. (**B**) The *2mFo − DFc* (Murshudov et al., 1997) electron density map at the aligned zinc center of the PGRP1, which is contoured at the sigma level of 1.0 and shown as *gray mesh*. (For interpretation of the references to color in this figure legend, the reader is referred to the Web version of this article.)

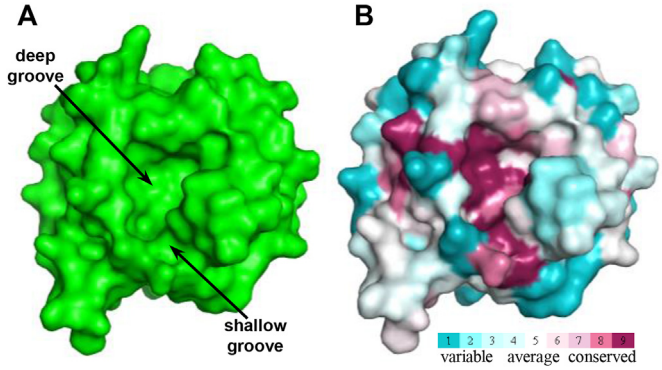

Fig. 5. A classical L-shaped PG-binding groove in *M. sexta* PGRP1. (**A**) Surface representation of the groove composed of an upper deep area and a lower shallow region. (**B**) Conservation of the surface residues depicted by a color gradient from *cyan* to *purple*. The conservation was calculated by ConSurf (http://consurf.tau.ac.il/ver3/index.html) using default settings (Landau et al., 2005). (For interpretation of the references to color in this figure legend, the reader is referred to the Web version of this article.)

(Fig. 7) but binds DAP-MPP preferably (Section 3.1) (Fig. 7). In addition, Arg254 of *Drosophila* PGRP-LE, whose guanidinium group formed a bidentate salt bridge with the ε-carboxyl group of DAP in TCT, was believed to be responsible for the DAP-PG recognition (Lim et al., 2006). This Arg residue, which constitutes a positively charged surface in the shallow groove, is highly conserved in DAP-type PGRPs, including *Drosophila* PGRP-LB, LCx and human PGRP-S, but not in Lys-type *Drosophila* PGRP-SA or human PGRP-Iα with similar binding activities to DAP- and Lys-PG monomers (Fig. 7A). *Drosophila* PGRP-SD possesses an Arg at this site and it binds to insoluble DAP-PGs from *B. subtilis* (Leone et al., 2008). In *M. sexta* PGRP1, this Arg residue is substituted by a completely buried residue Ser80, unlikely for any charge-charge interaction with DAP (Fig. 7A). These observations points to the possibility that additional mechanism contributes to the preferred binding of DAP-MPP to the PGRP1.

We attempted to co-crystallize the PGRP1 (0.37 mM) with DAP-PG (0.47 mM) and expected 99.4% of the protein in a ligand-bound state based on the K_d of 0.57 μM. However, the crystal did not contain the ligand since the entrance to the PG-bind groove of one molecule was shielded by the C-terminal α-helix of a symmetry-related molecule (data not shown). In order to understand the binding mechanism of *M. sexta* PGRP1, we then carried out a docking analysis using DAP- and Lys-MPPs as ligands. After selecting certain residues at the PG-binding groove as flexible to accommodate protein dynamics upon ligand binding, we successfully docked the ligands into the groove, each with ten possible conformations. Among them, the classical PG-binding patterns with the glycan moiety anchored in the deep area and the stem peptide extending to the shallow region were detected for both ligands (Fig. 8A and B). DAP-MPP is stabilized by 17 residues within 4.5 Å, with a docking energy of −5.34 kcal/mol, whereas Lys-MPP is stabilized by 21 residues with a slightly lower docking energy of −6.04 kcal/mol. Both bound ligands are mainly stabilized by hydrogen bonding and electrostatic interactions. For DAP-MPP, Tyr90 stabilizes the C-

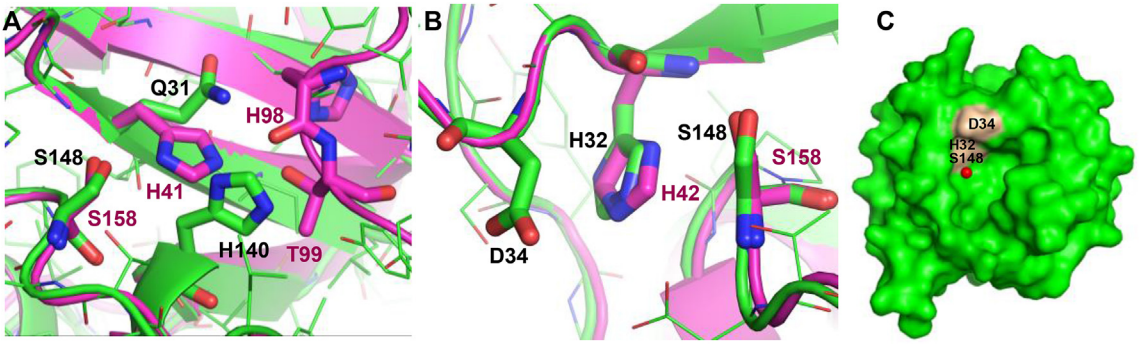

Fig. 4. M. *sexta* PGRP1 may possess a serine hydrolase activity. (**A**) Overlaying the PGRP1 (*green*) with *Drosophila* PGRP-SA (*magenta*) indicates the modified catalytic site does not exist in *M. sexta* PGRP1. Residues comprising the presumed catalytic triad of PGRP-SA are shown as *sticks*, along with those aligned in the PGRP1. (**B**) Superposition of the PGRP1 (*green*) with *Drosophila* PGRP-SA (*magenta*) at another putative catalytic site. The respective Ser/His dyads and Asp34 of the PGRP1 are shown as *sticks*. (**C**) Surface representation of *M. sexta* PGRP1, with Ser148, His32 and Asp34 *tinted*. These residues, located on the top of the PG-binding groove, are exposed to the solvent. The water molecule, which aligns to the Zn^{2+} ion of catalytic PGRPs, is shown as a *red sphere*. (For interpretation of the references to color in this figure legend, the reader is referred to the Web version of this article.)

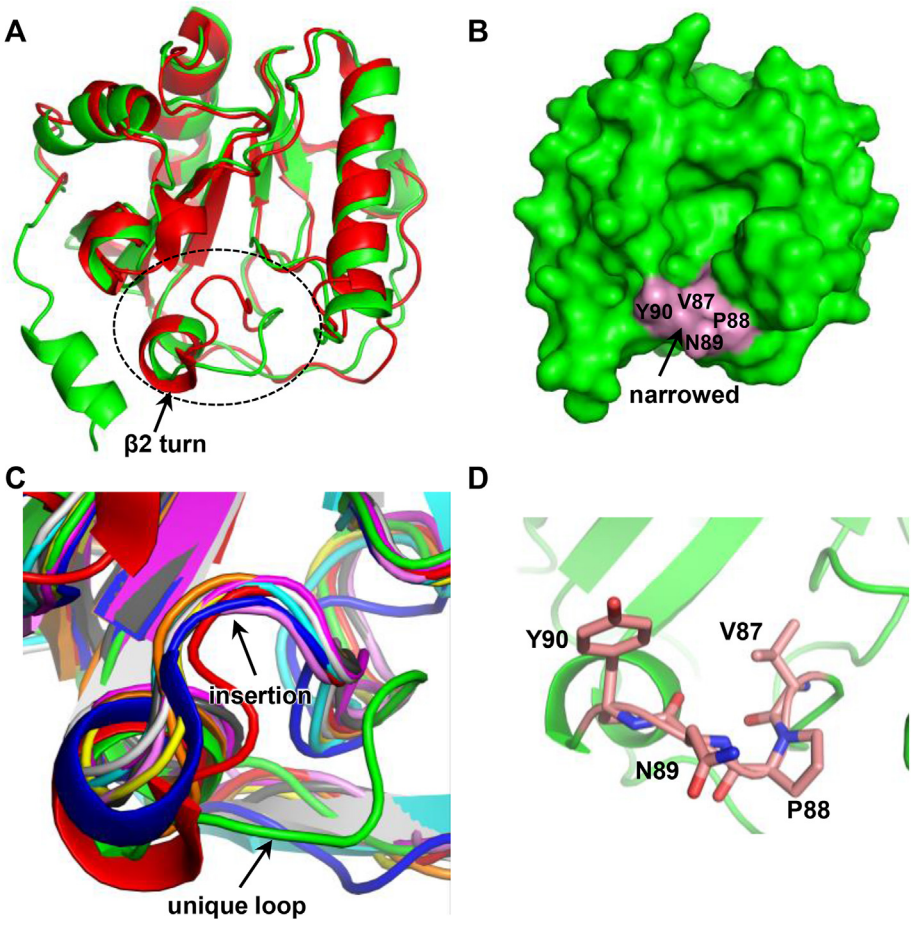

Fig. 6. A unique loop at the shallow region of the PG-binding groove in *M. sexta* PGRP1. (**A**) Secondary structure superposition of the PGRP1 (*green*) with *Drosophila* PGRP-LCa ectodomain (*red*). Conformational difference at the loop preceding β2 turn is indicated by a *dashed circle*. (**B**) Surface representation of Val87 – Tyr90 in the PGRP1. The shallow region is narrowed but undisrupted. (**C**) Structural alignment of the loop regions in *M. sexta* PGRP1 (*green*), *Drosophila* PGRP-LB (*cyan*), -LCa ectodomain (*red*), -LCx (*yellow*), -LE (*silver*), -SA (*magenta*), -SD (*blue*), human PGRP-S (*orange*), -Iα (*dark gray*), and -Iβ (*violet*). The black arrows indicate an insertion of the PGRP-LCa ectodomain (*red*) and a unique loop in the PGRP1. (**D**) Identification of Val87, Pro88, Asn89, and Tyr90 (shown as *sticks*) that form the unique loop region in *M. sexta* PGRP1. (For interpretation of the references to color in this figure legend, the reader is referred to the Web version of this article.)

terminus of the stem peptide through hydrogen bonding, whereas Asn89 binds DAP (Fig. 8C). Sequence alignment indicates that this Asn is unique in *M. sexta* PGRP1 but not the other PGRPs (Fig. 7A). For Lys-MPP, the Lys residue in the stem peptide is not involved in the interaction with any other atom in the complex, whereas the peptide is stabilized by Gln31, Lys98 and His140 in the deep area through hydrogen bonding (Fig. 8D).

It is intriguing that Lys-MPP have lower docking energy for PGRP1 binding but higher dissociation constant (45.58 vs. 0.57 μM) than DAP-MPP. One possibility is that the bound Lys-MPP is favorably hydrolyzed by PGRP1, leading to the dissociation of Lys-MPP fragments from PGRP1. For instance, *Drosophila* PGRP-SA possesses an unusual *L,D-*

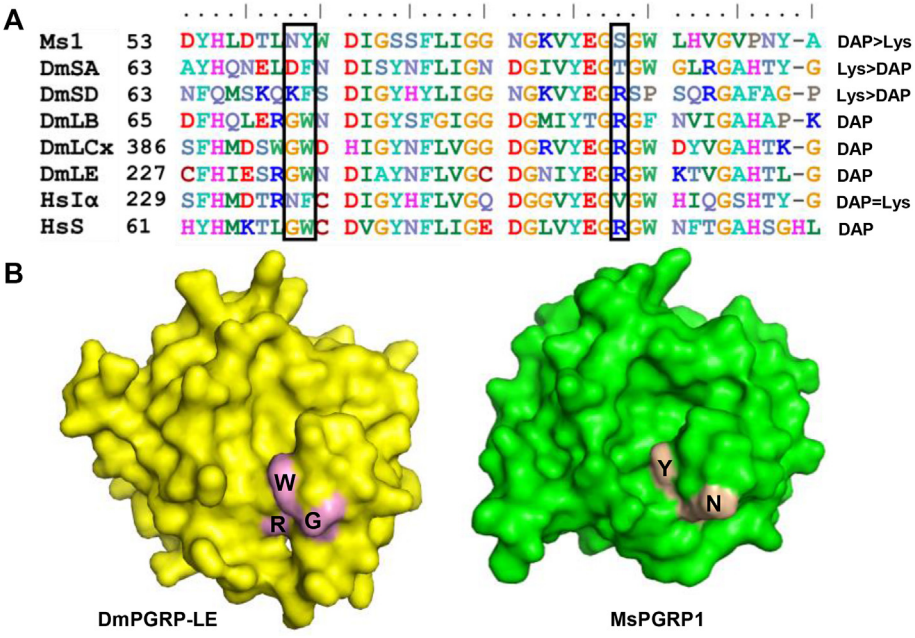

Fig. 7. Prediction of PG-interacting residues in the PGRP1 based on sequence analysis. (**A**) A part of the sequence alignment of *M. sexta* (Ms), *D. melanogaster* (Dm) and *Homo sapiens* (Hs) PGRPs, with their binding preferences indicated on the right. Sequence variations at the putative PG-recognition positions are marked by *black boxes*. (**B**) Surface representation of the potential DAP-PG interacting residues in *Drosophila* PGRP-LE and *M. sexta* PGRP1. Gly234, Trp235 and Arg254 (*pink*) of the PGRP-LE are located at the shallow groove, corresponding to Asn60, Tyr61 (*yellow*) and Ser80 (buried completely) of the PGRP1. (For interpretation of the references to color in this figure legend, the reader is referred to the Web version of this article.)

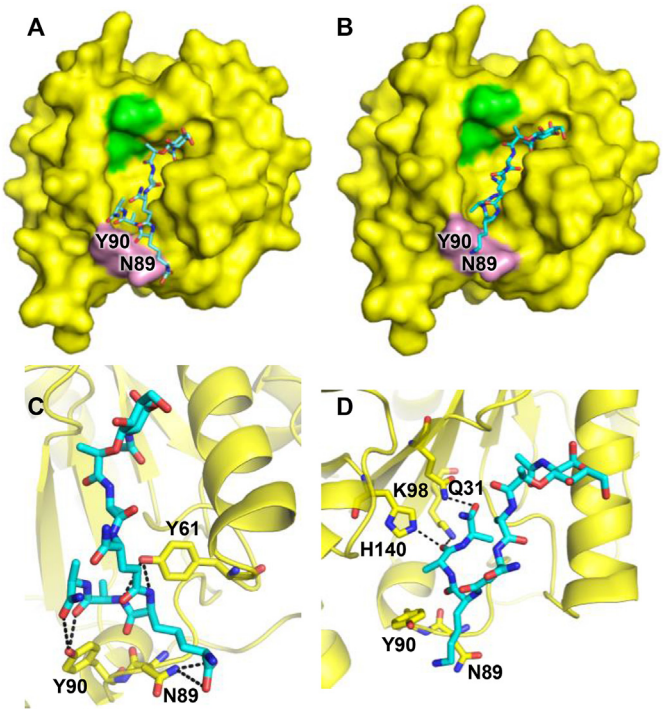

Fig. 8. M. *sexta* PGRP1 with the docked ligands in the classical binding mode. (**A**, **B**) Surface representation of the DAP-MPP (**A**) or Lys-MPP (**B**) binding in the PGRP1 groove. Side chains of Asn89 and Tyr90 (*pink*) are protruded from the surface. The putative catalytic site of PGRP1 is highlighted *green*. (**C**, **D**) Detailed illustrations of the critical molecular interactions between PGRP1 and DAP-MPP (**C**) or Lys-MPP (**D**). The hydrogen bonds are marked as *black* dashes. The ligands are shown as *cyan* sticks and *M. sexta* PGRP1 in *yellow*. (For interpretation of the references to color in this figure legend, the reader is referred to the Web version of this article.)

carboxypeptidase activity solely for DAP-type PGs (Chang et al., 2004), which may further explain why PGRP-SA preferentially responds to Lys-PGs for triggering the Toll pathway. The aforementioned docked ligands with the classical binding pattern are far away from the putative catalytic triad, however, a new type of binding conformations with lower docking energy is also detected for both DAP-MPP and Lys-MPP, in which the ligand is upside down, with the sugar moiety locked in the shallow groove and the stem peptide anchored to the deep area (Fig. S3). Asn89 and Tyr90 from the unique loop, which interferes with the ligand stem peptide in the classical binding pattern (Fig. 8C and D), firmly locks the sugar ring, possibly reducing the docking energy (−8.37 kcal/mol for DAP-MPP and −9.19 kcal/mol for Lys-MPP). Remarkably, the bound ligands with this novel binding pattern are close to the putative catalytic triad (Fig. S3), making them possible to be hydrolyzed by *M. sexta* PGRP1. Lys-MPP, which has a relatively lower docking energy than DAP-MPP in this binding mode, may have led to preferential hydrolysis by the PGRP1, resulting in more new mass peaks (Fig. S1).

3.6. Concluding remarks

In this preliminary study, we investigated the association of DAP- and Lys-MPPs and confirmed the previous binding result that *M. sexta* PGRP1 preferably interacts with DAP-peptidoglycan polymers. The PGRP1 crystal structure provides insights into new structural features, such as a putative catalytic site, a unique PG binding groove, and a possible non-GWR mechanism for distinguishing DAP- and Lys-PGs. The docking analysis implicated a drastically different binding pattern, energy levels, and structural properties (*e.g.*, unique β2-turn loop of Val87 − Tyr90). While the docking results are in nature highly speculative, they clearly indicate that our current knowledge on the differential recognition of DAP- and Lys-PGs is far from complete. Future research on the PGRP structure, function, and mechanism is necessary for a thorough understanding of this family of pattern recognition proteins with or without an enzymatic activity.

Data deposition

Atomic coordinates and structure factors have been deposited in the Protein Data Bank (www.rcsb.org) with PDB ID of 6CKH.

Acknowledgments

We gratefully acknowledge the staff of beam-line 19ID at the Advanced Photon Source for their support. This work was supported by National Institutes of Health Grants AI112662 and GM58634. Mass spectrometry analyses were performed in the DNA/Protein Resource Facility at Oklahoma State University. This article was approved for publication by the Director of the Oklahoma Agricultural Experiment Station and supported in part under projects OKL03054 and OKL03060.

Appendix A. Supplementary data

Supplementary data to this article can be found online at https://doi.org/10.1016/j.ibmb.2019.03.001.

References

Adams, P.D., Afonine, P.V., Bunkóczi, G., Chen, V.B., Davis, I.W., Echols, N., Headd, J.J., Hung, L.W., Kapral, G.J., Grosse-Kunstleve, R.W., McCoy, A.J., Moriarty, N.W., Oeffner, R., Read, R.J., Richardson, D.C., Richardson, J.S., Terwilliger, T.C., Zwart, P.H., 2010. PHENIX: a comprehensive Python-based system for macromolecular structure solution. Acta Crystallogr. D Biol. Crystallogr. 66 (Pt 2), 213–221.

Berman, H., Henrick, K., Nakamura, H., 2003. Announcing the worldwide protein data bank. Nat. Struct. Biol. 10, 980.

Bischoff, V., Vignal, C., Boneca, I.G., Michel, T., Hoffmann, J.A., Royet, J., 2004. Function of the *Drosophila* pattern-recognition receptor PGRP-SD in the detection of Gram-positive bacteria. Nat. Immunol. 5, 1175–1180.

Chang, C.I., Chelliah, Y., Borek, D., Mengin-Lecreulx, D., Deisenhofer, J., 2006. Structure of tracheal cytotoxin in complex with a heterodimeric pattern-recognition receptor. Science 311, 1761–1764.

Chang, C.I., Ihara, K., Chelliah, Y., Mengin-Lecreulx, D., Wakatsuki, S., Deisenhofer, J., 2005. Structure of the ectodomain of *Drosophila* peptidoglycan-recognition protein LCa suggests a molecular mechanism for pattern recognition. Proc. Natl. Acad. Sci. U.S.A. 102, 10279–10284.

Chang, C.I., Pili-Floury, S., Hervé, M., Parquet, C., Chelliah, Y., Lemaitre, B., Mengin-Lecreulx, D., Deisenhofer, J., 2004. A *Drosophila* pattern recognition receptor contains a peptidoglycan docking groove and unusual *L,D*-carboxypeptidase activity. PLoS Biol. 2, E277.

Chen, V.B., Arendall 3rd, W.B., Headd, J.J., Keedy, D.A., Immormino, R.M., Kapral, G.J., Murray, L.W., Richardson, J.S., Richardson, D.C., 2010. MolProbity: all-atom structure validation for macromolecular crystallography. Acta Crystallogr. D Biol. Crystallogr. 66 (Pt 1), 12–21.

Cheng, X., Zhang, X., Pflugrath, J.W., Studier, F.W., 1994. The structure of bacteriophage T7 lysozyme, a zinc amidase and an inhibitor of T7 RNA polymerase. Proc. Natl. Acad. Sci. U.S.A. 91, 4034–4038.

Cho, S., Wang, Q., Swaminathan, C.P., Hesek, D., Lee, M., Boons, G.J., Mobashery, S., Mariuzza, R.A., 2007. Structural insights into the bactericidal mechanism of human peptidoglycan recognition proteins. Proc. Natl. Acad. Sci. U.S.A. 104, 8761–8766.

Chowdhury, A.R., Boons, G.J., 2005. The synthesis of diaminopimelic acid containing peptidoglycan fragments using metathesis cross coupling. Tetrahedron Lett. 46, 1675–1678.

DeLano, W.L., 2002. The PyMOL Molecular Graphics System. DeLano Scientific, Palo Alto, CA, USA.

Deng, J., Davies, D.R., Wisedchaisri, G., Wu, M., Hol, W.G., Mehlin, C., 2004. An improved protocol for rapid freezing of protein samples for long-term storage. Acta Crystallogr. D Biol. Crystallogr. 60 (Pt 1), 203–204.

Dziarski, R., 2004. Peptidoglycan recognition proteins (PGRPs). Mol. Immunol. 40, 877–886.

Dziarski, R., Gupta, D., 2006. The peptidoglycan recognition proteins (PGRPs). Genome Biol. 7, 232.

Emsley, P., Lohkamp, B., Scott, W.G., Cowtan, K., 2010. Features and development of coot. Acta Crystallogr. D Biol. Crystallogr. 66 (Pt 4), 486–501.

Gelius, E., Persson, C., Karlsson, J., Steiner, H., 2003. A mammalian peptidoglycan recognition protein with *N*-acetylmuramoyl-*L*-alanine amidase activity. Biochem. Biophys. Res. Commun. 306, 988–994.

Guan, R., Brown, P.H., Swaminathan, C.P., Chowdhury, A.R., Boons, G.J., Mariuzza, R.A.,

2006. Crystal structure of human peptidoglycan recognition protein Iα bound to a muramyl pentapeptide from Gram-positive bacteria. Protein Sci. 15, 1199–1206.
Guan, R., Mariuzza, R.A., 2007. Peptidoglycan recognition proteins of the innate immune system. Trends Microbiol. 15, 127–134.
Guan, R., Chowdhury, A.R., Ember, B., Kumar, S., Boons, G.J., Mariuzza, R.A., 2004. Structural basis for peptidoglycan binding by peptidoglycan recognition proteins. Proc. Natl. Acad. Sci. U.S.A. 101, 17168–17173.
Heaton, W.A., Good, C.E., Galloway-Haskins, R., Yomtovian, R.A., Jacobs, M.R., 2014. Evaluation of a rapid colorimetric assay for detection of bacterial contamination in apheresis and pooled random-donor platelet units. Transfusion 54, 1634–1641.
Jiang, H., Vilcinskas, A., Kanost, M.R., 2010. Immunity in lepidopteran insects. Adv. Exp. Med. Biol. 708, 181–204.
Kaneko, T., Goldman, W.E., Mellroth, P., Steiner, H., Fukase, K., Kusumoto, S., Harley, W., Fox, A., Golenbock, D., Silverman, N., 2004. Monomeric and polymeric Gram-negative peptidoglycan but not purified LPS stimulate the *Drosophila* IMD pathway. Immunity 20, 637–649.
Kanost, M.R., Jiang, H., 2015. Clip-domain serine proteases as immune factors in insect hemolymph. Curr. Opin. Insect Sci. 11, 47–55.
Kim, M.S., Byun, M., Oh, B.H., 2003. Crystal structure of peptidoglycan recognition protein LB from *Drosophila melanogaster*. Nat. Immunol. 4, 787–793.
Kumar, S., Chowdhury, A.R., Ember, B., Wang, Q., Guan, R., Mariuzza, R.A., Boons, G.J., 2005. Selective recognition of synthetic lysine and meso-diaminopimelic acid-type peptidoglycan fragments by human peptidoglycan recognition proteins Iα and S. J. Biol. Chem. 280, 37005–37012.
Kurata, S., 2014. Peptidoglycan recognition proteins in *Drosophila* immunity. Dev. Comp. Immunol. 42, 36–41.
Landau, M., Mayrose, I., Rosenberg, Y., Glaser, F., Martz, E., Pupko, T., Ben-Tal, N., 2005. ConSurf: the projection of evolutionary conservation scores of residues on protein structures. Nucleic Acids Res. 33, W299–W302.
Lemaitre, B., Hoffmann, J., 2007. The host defense of *Drosophila melanogaster*. Annu. Rev. Immunol. 25, 697–743.
Leone, P., Bischoff, V., Kellenberger, C., Hetru, C., Royet, J., Roussel, A., 2008. Crystal structure of *Drosophila* PGRP-SD suggests binding to DAP-type but not Lys-type peptidoglycan. Mol. Immunol. 45, 2521–2530.
Lim, J.H., Kim, M.S., Kim, H.E., Yano, T., Oshima, Y., Aggarwal, K., Goldman, W.E., Silverman, N., Kurata, S., Oh, B.H., 2006. Structural basis for preferential recognition of diaminopimelic acid-type peptidoglycan by a subset of peptidoglycan recognition proteins. J. Biol. Chem. 281, 8286–8295.
Mellroth, P., Karlsson, J., Steiner, H., 2003. A scavenger function for a *Drosophila* peptidoglycan recognition protein. J. Biol. Chem. 278, 7059–7064.
Michel, T., Reichhart, J.M., Hoffmann, J.A., Royet, J., 2001. *Drosophila* Toll is activated by Gram-positive bacteria through a circulating peptidoglycan recognition protein. Nature 414, 756–759.
Minor, W., Cymborowski, M., Otwinowski, Z., Chruszcz, M., 2006. HKL-3000: the integration of data reduction and structure solution – from diffraction images to an initial model in minutes. Acta Crystallogr. D Biol. Crystallogr. 62 (Pt 8), 859–866.
Morris, G.M., Huey, R., Lindstrom, W., Sanner, M.F., Belew, R.K., Goodsell, D.S., Olson, A.J., 2009. AutoDock4 and AutoDockTools4: automated docking with selective receptor flexibility. J. Comput. Chem. 30, 2785–2791.
Murshudov, G.N., Vagin, A.A., Dodson, E.J., 1997. Refinement of macromolecular structures by the maximum-likelihood method. Acta Crystallogr. D Biol. Crystallogr. 53, 240–255.
Reiser, J.B., Teyton, L., Wilson, I.A., 2004. Crystal structure of the *Drosophila* peptidoglycan recognition protein (PGRP)-SA at 1.56 Å resolution. J. Mol. Biol. 340, 909–917.
Strand, M.R., 2008. The insect cellular immune response. Insect Sci. 15, 1–14.
Sumathipala, N., Jiang, H., 2010. Involvement of *Manduca sexta* peptidoglycan recognition protein-1 in the recognition of bacteria and activation of prophenoloxidase system. Insect Biochem. Mol. Biol. 40, 487–495.
Swaminathan, C.P., Brown, P.H., Chowdhury, A.R., Wang, Q., Guan, R., Silverman, N., Goldman, W.E., Boons, G.J., Mariuzza, R.A., 2006. Dual strategies for peptidoglycan discrimination by peptidoglycan recognition proteins (PGRPs). Proc. Natl. Acad. Sci. U.S.A. 103, 684–689.
Takehana, A., Katsuyama, T., Yano, T., Oshima, Y., Takada, H., Aigaki, T., Kurata, S., 2002. Overexpression of a pattern-recognition receptor, peptidoglycan-recognition protein-LE, activates imd/relish-mediated antibacterial defense and the prophenoloxidase cascade in *Drosophila* larvae. Proc. Natl. Acad. Sci. U.S.A. 99, 13705–13710.
Vollmer, W., Blanot, D., de Pedro, M.A., 2008. Peptidoglycan structure and architecture. FEMS Microbiol. Rev. 32, 149–167.
Wang, Y., Jiang, H., 2017. Prophenoloxidase activation and antimicrobial peptide expression induced by the recombinant microbe binding protein of *Manduca sexta*. Insect Biochem. Mol. Biol. 83, 35–43.
Wang, Z.M., Li, X., Cocklin, R.R., Wang, M., Wang, M., Fukase, K., Inamura, S., Kusumoto, S., Gupta, D., Dziarski, R., 2003. Human peptidoglycan recognition protein-L is an *N*-acetylmuramoyl-*L*-alanine amidase. J. Biol. Chem. 278, 49044–49052.
Werner, T., Liu, G., Kang, D., Ekengren, S., Steiner, H., Hultmark, D., 2000. A family of peptidoglycan recognition proteins in the fruit fly *Drosophila melanogaster*. Proc. Natl. Acad. Sci. U.S.A. 97, 13772–13777.
Zaidman-Remy, A., Hervé, M., Poidevin, M., Pili-Floury, S., Kim, M.S., Blanot, D., Oh, B.H., Ueda, R., Mengin-Lecreulx, D., Lemaitre, B., 2006. The *Drosophila* amidase PGRP-LB modulates the immune response to bacterial infection. Immunity 24, 463–473.
Zhang, X., He, Y., Cao, X., Gunaratna, R.T., Chen, Y.R., Blissard, G., Kanost, M.R., Jiang, H., 2015. Phylogenetic analysis and expression profiling of the pattern recognition receptors: insights into molecular recognition of invading pathogens in *Manduca sexta*. Insect Biochem. Mol. Biol. 62, 38–50.